Infrared lines as probes of solar magnetic features

II. Diagnostic capabilities of Fe I 15648.5 Å and 15652.9 Å

S.K. Solanki[1], I. Rüedi[1] and W. Livingston[2]

[1] Institute of Astronomy, ETH-Zentrum, CH-8092 Zürich, Switzerland
[2] National Solar Observatory, NOAO*, P.O. Box 26732, Tucson, AZ 85726, USA

Abstract. The properties of two Fe I lines at 15648.5 Å and 15652.9 Å in the infrared H-band are investigated using numerical radiative transfer calculations. It is shown that using this combination of a Landé $g = 3$ and a $g_{eff} = 1.53$ line it is possible to measure the field strength in solar magnetic features simply and with great accuracy. The $g = 3$ line alone allows field strengths as low as 300–600 G to be measured (depending on the type of magnetic feature). By forming the line ratio between the V profiles of these lines it is, in principle, possible to measure field strengths as low as 100 G, thus achieving a sensitivity otherwise only possible with the emission lines near 12μ. Other diagnostic capabilities of these lines are also analysed (e.g. of temperature and magnetic inclination angle). Calibration curves for measuring the field strength and the magnetic inclination angle are given. Some initial, illustrative comparisons are made with observed profiles. Thus it is shown that magneto-optical effects cannot explain the inversions in the cores of some observed Stokes V profiles.

Key words: solar magnetic fields – flux tubes – sunspots – infrared polarimetry

1. Introduction

In Paper I of the present series (Muglach & Solanki 1991) the Stokes V profiles of all the unblended Fe I lines in the infrared H-band (1.5–1.8μ) were analysed statistically. In the present paper we consider two of these lines, Fe I 15648.5 Å and Fe I 15652.9 Å, in greater detail. We study and develop the potential of these two lines to diagnose properties of solar magnetic features, foremost of all the magnetic field strength. In Papers III (Rüedi et al. 1992a), IV (Rüedi et al. 1992b) and V (Solanki et al. 1992) we apply the diagnostics explored here to profiles of these lines observed in solar plages and sunspots.

The need for a careful evaluation of the properties of these lines is keenly felt. Fe I 15648.5 Å is a Zeeman triplet with a Landé factor g of 3. It is the best-known spectral line in the H-band, having been observed and analysed in the sun by Harvey &

Hall (1975), Harvey (1977), Sun et al. (1987), Stenflo et al. (1987), Zayer et al. (1989), Livingston (1991), Rabin et al. (1991) and Rabin (1992). Additionally, it has been used to measure stellar magnetic fields by Giampapa et al. (1983) and Gondoin et al. (1985). Its popularity rests on its substantial Zeeman sensitivity, which is approximately 3 times that of the $g = 3$ line at 5250.2 Å. In particular, it allows the kG fields present in most small-scale magnetic structures to be measured directly from its Zeeman splitting, e.g. from the wavelength difference between its Stokes V peaks. As such, its potential as a diagnostic of magnetic field strengths has only just begun to be realized, and it will certainly find widespread use in the future (see, e.g., the Near Infrared Magnetograph, NIM, project described by Rabin et al. 1991). However, in spite of its undoubted importance there has been no systematic study of its properties based on radiative transfer calculations.

The other line, Fe I 15652.9 Å, is considerably less well known, and was until recently even misidentified (see Johansson & Learner 1990; Solanki et al. 1990). The best currently known atomic parameters of the two lines are given in Table 1, where χ_e is the excitation potential of the lower level. The weighted logarithmic oscillator strengths $\log(g^\star f)$ have been determined by fitting profiles observed in a region with no detectable magnetic flux. An iron abundance of 7.56 on a logarithmic scale with a hydrogen abundance of 12 was assumed.

Table 1. Line parameters

Line	Transition	g_{eff}	χ_e [eV]	$\log(g^\star f)$
Fe I 15648.518	$e^7D_1 - 3d^64s5p\,^7D_1^0$	3	5.43	–0.7
Fe I 15652.889	$f^7D_5 - (9/2)[7/2]_4^0$	1.53	6.25	–0.095

A glance at the table shows that the second line has no extraordinary properties. In spite of the difference in $\log(g^\star f)$ the two lines have a similar strength in the quiet sun (see Fig. 1). The main reason we are considering it together with the $g = 3$ line is the relative proximity in wavelength and the similarity of the two lines, with the exception of their Landé factors. The former property allows the two lines to be observed simultaneously with a grating spectrograph and even a relatively small array detector

* Operated by the Association of Universities for Research in Astronomy, Inc. (AURA) under cooperative agreement with the National Science Foundation.
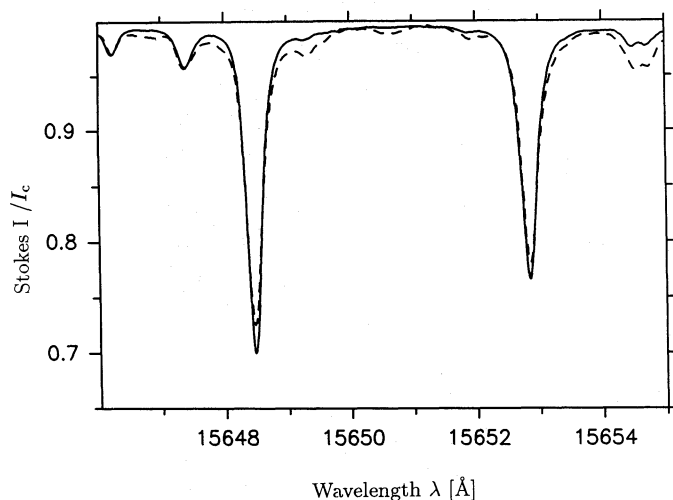
Fig. 1. Stokes I profiles of Fe I 15648.5 Å and 15652.9 Å observed in the quiet sun. Solid curves: Extract from the spectral atlas of Delbouille et al. (1981) obtained with a Fourier transform spectrometer (FTS) at a resolving power of 400 000. Dashed curve: Spectrum obtained by Livingston (1991) with a grating spectrograph

(Rabin et al. 1991), the latter implies that the $g_{eff} = 1.53$ line can be used to constrain the turbulent velocity broadening of the $g = 3$ line and thus allow field strength gradients to be inferred (Zayer et al. 1989). However, as we shall see, the combination of two such lines has further advantages.

The Stokes I (i.e. unpolarized intensity) profiles of both lines are plotted in Fig. 1. The solid curve corresponds to profiles measured in the quiet sun by Delbouille et al. (1981) using the McMath main telescope on Kitt Peak and a Fourier transform spectrometer (FTS) with an approximate spectral resolving power of 400 000. The dashed spectrum was obtained by Livingston (1991), also in a quiet region, using the same telescope, but the main grating spectrograph and the "Baboquivari" detector of Hall (1974). Such grating spectrograph data are used in the present paper and in papers III and V. The spectral resolving power of these spectra is 150 000. It is determined by convolving the Delbouille et al. spectrum with Gaussian instrumental profiles of different widths until one of the broadened profiles matches the profiles observed with the grating spectrograph. The spectrograph was used in double-pass mode which virtually eliminates stray light. This is confirmed by the comparison with the atlas profiles of Delbouille et al. (1981). The rms noise lies in the range 1–3 × 10$^{-3}I_c$ (I_c is the continuum intensity). It is determined using the method described by Zayer et al. (1990). More information on the instrumental setup and the observing technique is given by Livingston (1991). Note that for the analysed observations both polarizations were measured consecutively at each wavelength during the scan over the observed wavelength interval. Each analysed spectrum is composed of a series (10–20) wavelength scans averaged together in order to average over any drifts due to seeing. The signal-to-noise ratio is improved by approximately a factor of 2 by Fourier filtering the highly oversampled spectra before analysis.

In Sect. 2 we present the models we have used for our radiative transfer calculations. Sect. 3 contains the results of a series of calculations based on height-independent magnetic fields, while Sect. 4 outlines the results of calculations based on thin-tube models. Conclusions are drawn in Sect. 5.

2. Models

2.1. Model atmospheres

We have used 6 different empirical models to describe the atmospheres in which the line transfer calculations are carried out. Their photospheric temperature stratifications T as a function of continuum optical depth τ at 16000 Å are shown in Fig. 2. The coolest model used here is the umbral model M of Maltby et al. (1986), abbreviated here by MALTM. It describes the dark umbral background in the middle phase of the sunspot cycle. The second coolest model is the penumbral model of Ding & Fang (1989), abbreviated as DF. It is a relatively cool penumbral model and may best describe the inner penumbra. There follows the umbral warm-component model of Obridko & Staude (1988), denoted here by OS2. It is meant to represent umbral dots, but is probably also a reasonable representation of the outer parts of the penumbra and possibly of small pores, at least in the limited height range over which the analysed lines are formed. Next is the quiet sun model of Gingerich et al. (1971), extended downwards into the convection zone by Spruit (1974). The combined model is referred to as the HSRASP. This relatively old model is employed instead of more recent ones since the two models of small flux tubes we use (described below) were constructed using the HSRASP as reference. The cooler of the 2 small-flux-tube atmospheres (Solanki 1986) describes magnetic features in an active plage region (PLA), while the hotter one describes magnetic features in a network region (NET). We use these models instead of the newer empirical models of Keller et al. (1990) since the former reproduce the profile of the $g = 3$ Fe I 15648.5 Å line without requiring any additional horizontal distribution of field strengths (Zayer et al. 1989, Zayer 1990).
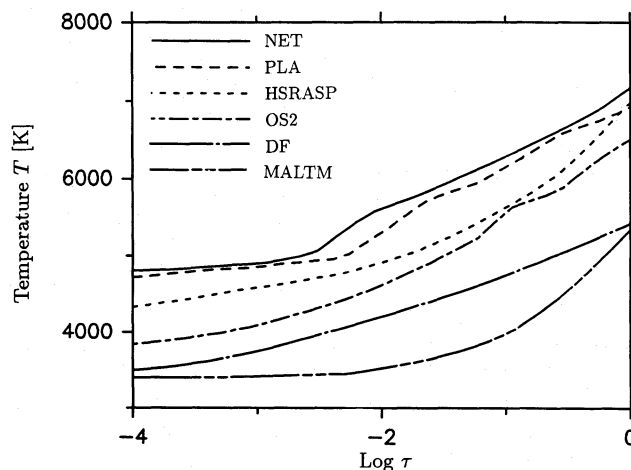

Fig. 2. Temperature T vs. logarithmic continuum optical depth log τ at 16000 Å of the 6 model atmospheres used in the main part of the present investigation. The various curves are identified in the figure. More details about each model (NET, PLA, HSRASP, OS2, DF, MALTM) are given in the text

2.2. Magnetic structure and radiative transfer

First we carried out a series of calculations assuming the field to be constant with height. This is a reasonable assumption for sunspots due to their small vertical field strength gradients. Also,

314

in contrast to self-consistent flux-tube models, it allows effects due to the field strength to be easily separated from those due to field-strength gradients, the Wilson depression (hot walls), etc. Finally, the line profiles in such a model need only be calculated along a single ray.

The line transfer calculations presented in this series of papers are in LTE, which provides an excellent approximation of the physics of formation of these high-excitation, low height-of-formation lines. The numerics of the line transfer are handled by the DELO (Diagonal Element Lambda Operator) technique of Rees et al. (1989), with elements of a code described by Murphy (1990) and Murphy & Rees (1990).

Later we repeat a number of the test calculations for flux-tube models satisfying horizontal (and vertical) pressure balance in the thin-tube approximation and magnetic flux conservation. For small flux tubes the thin-tube approximation reproduces solutions of the full MHS or MHD equations rather well (Knölker et al. 1988; Steiner & Pizzo 1989). To treat the effects of the flux-tube expansion with height properly we calculate the line profiles along 10 vertical rays passing through the flux tube at different radial distances from its axis. The radial spacing of the rays follows that outlined by Solanki & Roberts (1992). The contributions of the individual rays are weighted by the surface area represented by each ray and added together to give the line profile of the spatially unresolved flux tube. The line profiles resulting from these calculations, although more realistic for solar plages, are also more difficult to interpret than profiles formed in a homogeneous field. Therefore, we briefly discuss some of the properties of these models which are relevant for the interpretation of the calculated line profiles.

The magnetic field of each thin, vertical flux-tube model is described by two parameters, the field strength B at a given height z_0 and the magnetic filling factor α at z_0 (describing the fraction of the surface at z_0 covered by a field $B(z_0)$. Both B and α vary with height and only the product of αB is constant. An increase in $B(z_0)$ is achieved by shifting the internal atmosphere downwards by a Wilson depression Z_w until the desired $p_{int}(z_0)$ is obtained. Although $B(z_0)$ and $\alpha(z_0)$ are physically sensible parameters, they are not related in a simple manner to the B and α at the height of Stokes V formation (e.g. Steiner & Pizzo 1989). For a given line the formation height in turn depends on the temperature within the flux tube (and to a lesser extent also in its surroundings), as well as on $B(z_0)$ itself. For the relatively simple case of a fixed temperature and $\alpha(z_0)$, let us briefly consider the effect of varying $B(z_0)$ between 0 and a maximum value corresponding to a completely evacuated flux tube. As $B(z_0)$ is increased the $\tau_{int} = 1$ level moves steadily downwards, implying that the lines are formed at greater and greater geometrical depth, where the field strength can become considerably larger than at $z = 0$. This effect is illustrated in Fig. 3a, where $B(\tau_{int} = 1)$ is plotted against $B(z = 0)$ for 2 different atmospheres within the flux tubes, HSRASP (solid) and PLA (dashed). The external atmosphere is the HSRASP in both cases. Note how $B(\tau_{int} = 1)$ continues increasing, although $B(z = 0)$ approaches its maximum value: $B_{max} \approx 1800$ G for the HSRASP. However, since we have fixed $\alpha(z_0)$, the α at the height of line formation (and therefore the amplitudes of V, Q and U) decreases steadily as $B(\tau_{int} = 1)$ increases.

Note that although $B(\tau_{line})$ always increases with increasing $B(z_0)$ (τ_{line} is the τ of line formation), this need not always be the case for $dB(\tau)/d\tau$ at $\tau = \tau_{line}$. The field-strength gradient depends on the difference between the external and internal pressure scale

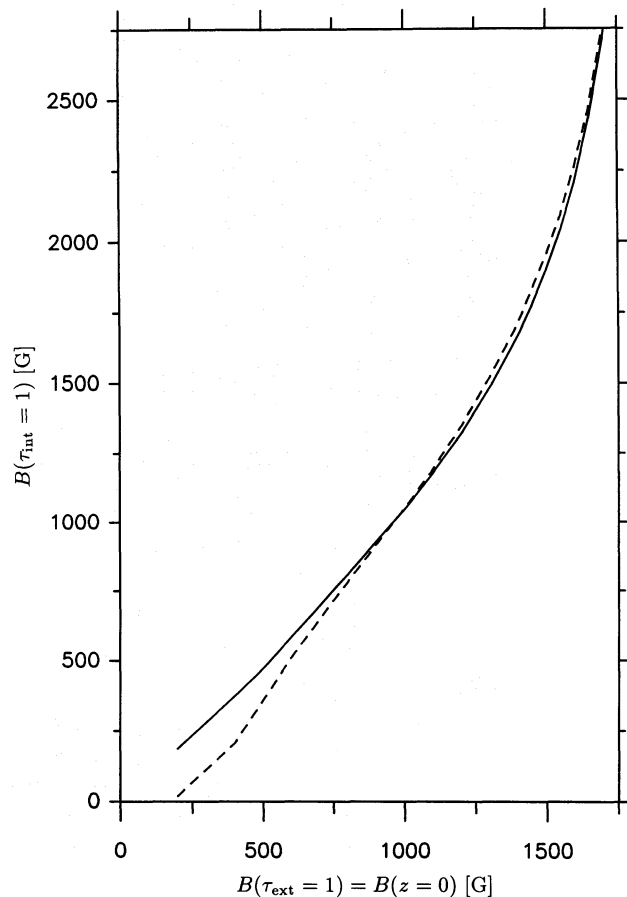**Fig. 3a.** Thin-tube field strength, B, at unit continuum optical depth within the flux tube, $\tau_{int} = 1$, vs. B at unit continuum optical depth in the external atmosphere, $\tau_{ext} = 1$, which corresponds to the origin of the geometrical height scale ($z = 0$). Solid curve: the flux tube atmosphere is represented by the HSRASP model, dashed curve: PLA model. The non-magnetic atmosphere corresponds to the HSRASP in both cases

heights and thus depends sensitively on the external and internal temperature structure. Figure 3b illustrates that the vertical gradient of the field strength is not necessarily monotonic.

One point which may cause some confusion in Fig. 3a is that for $B(z = 0) \lesssim 700$ G in the PLA model (dashed) $B(\tau_{int} = 1)$ is actually smaller than $B(z = 0)$. The higher temperature in the PLA model increases its continuum opacity relative to the HSRASP, so that for small $B(z = 0)$ the $\tau = 1$ level in the flux tube can lie higher than the $\tau = 1$ level in the quiet sun. This is illustrated in Fig. 3b [lowest dashed curve, PLA model with $B(\tau_{int} = 1) = 500$ G], where $B(z)$ is plotted for three different $B(\tau = 1)$ values. For a discussion of the behaviour of $B(z)$ for $z \gtrsim 100$ km of the PLA/HSRASP model with $B(\tau_{int} = 1) = 500$ G see Sect. 4.1. However, we don't expect this to be the case in nature, since for small field strengths the internal and external atmospheres are expected to be relatively similar. Therefore the HSRASP probably provides a better representation of reality for $B(z = 0) \lesssim 700$ G.
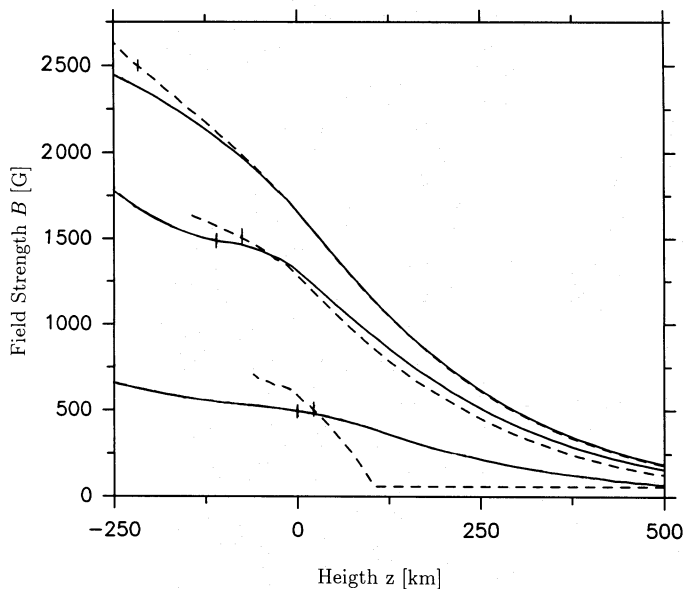
Fig. 3b. B vs. geometrical height z for the same atmospheres as in Fig. 3a. From top to bottom the three sets of curves correspond to $B(\tau_{int} = 1) = 2500$ G, $B(\tau_{int} = 1) = 1500$ G, and $B(\tau_{int} = 1) = 500$ G, respectively. The $\tau_{int} = 1$ levels are indicated by small vertical tickmarks in the relevant curves

3. Results based on models with height-independent fields

For each of the six model atmospheres (Sect. 2.1) we have calculated the Stokes profiles of both lines for field strengths ranging between 100 G and 2500 G, for inclination angles γ between $0°$ and $90°$, for macroturbulences between 0 and 4 km/s and for fudge factor δ_Γ to Unsöld's (1955) formula for Van der Waal's damping constant between 1.5 and 2.5. A selected set of Stokes V profiles for 100, 500, 1000, 1500, 2000 and 2500 G at $\gamma = 0°$ in the hottest and coolest of the six atmospheres, NET and MALTM, are shown in Fig. 4. In the following we discuss various aspects of the resulting profiles.

3.1. Temperature dependence

A comparison between Figs. 4a and 4c or between 4b and 4d shows that inspite of their high χ_e values the two lines do change with temperature. They grow stronger and become saturated as the temperature is lowered. However, considering that the temperature difference between the two models is 2000–2500 K the change in the line profiles is not overly large (cf. Paper I). The lines change mainly in equivalent width and relatively little in line depth. For example, the $g = 3$ line changes by a factor of 5.44 in equivalent width between NET and MALTM, but only by a factor of 2 in depth. This has partly to do with the small temperature sensitivity of the Planck function near 1.5μ and partly with the small temperature gradient of the MALTM atmosphere (lines calculated in the DF model are slightly deeper). For each of the six models Table 2 lists the equivalent widths W_λ of the two lines, the ratio of their equivalent widths and the ratio of their depths. All values are for $B = 0$. The dependence of the depth- and W_λ-ratios on temperature is due to the difference in χ_e of the two lines. We confirmed the qualitative form of the temperature dependence by comparing spectra obtained in bright plages, a pore, sunspot penumbrae and umbrae.

Table 2. Temperature dependence

Model	$T(\tau = 1)$ [K]	ratio of depths 15648/15652	W_λ [mÅ] 15648	W_λ [mÅ] 15652
NET	7203	1.24	36	32
PLA	6923	1.31	42	36
HSRASP	6977	1.33	88	79
OS2	6508	1.46	89	73
DF	5428	1.56	119	98
MALTS	5348	2.25	196	135

For resolved magnetic features the equivalent width of either line serves as a diagnostic of the temperature, but for unresolved features only the considerably less sensitive ratios can be reliably used. The different temperature sensitivities of the two lines reflect their different excitation potentials. The slightly smaller W_λ of Fe I 15652.9 Å in the cooler OS2 model than in the HSRASP is due to the different temperature gradients in the models. This additional sensitivity to temperature gradients further complicates the issue, so that these two lines can serve only in a very limited manner as temperature diagnostics, except possibly in relatively cool atmospheres (note the large change in the depth and W_λ ratios between the DF and MALTM atmospheres). However, at low temperatures blends due to molecular lines (3–1 band of OH, L. Wallace, private communication) can seriously affect the profile of the 15652.9 Å line.

On the other hand, the limited temperature sensitivity of the two lines is a boon if they are used to measure field strengths, field strength gradients and magnetic filling factors. In particular, the relatively similar equivalent widths and line depths of the two lines in the temperature range covered by NET to OS2 suggests that the same broadening velocity (macroturbulence) can be used for both, thus allowing magnetic field distributions and gradients to be determined (see Zayer et al. 1989).

In the coolest atmosphere, MALTM, the value of the fudge factor to the Van der Waal's damping constant, δ_Γ, plays a substantial role in determining the line profile shapes. This can have important consequences for the derived magnetic field strength distributions, in particular in cool umbrae, since then only the $g = 3$ line can be used, the $g_{eff} = 1.53$ line being almost completely obliterated by strong, Zeeman-sensitive, molecular blends. As an illustration consider Fig. 5, which shows the Stokes V profile of the $g = 3$ line, as observed in the darkest part of the umbra of a large sunspot (solid curve, note the many weak blends due to molecular lines) and as calculated using the MALTM model and a distribution of field strengths centred on 3500 G. The complete observed spectrum, including the wavelength over which the $g_{eff} = 1.53$ line is seen in warmer atmospheres, is shown in panel 9 (Fig. 2) of Livingston (1991). A fit of the quality shown in Fig. 5 can be obtained with any δ_Γ between 1.5 and 2.5, which are typical δ_Γ values expected for high-excitation lines (Holweger 1979; Simmons & Blackwell 1982).[1]

However, in order to reproduce the observed profile using the MALTM atmosphere the σ-components of the synthetic profiles

---

[1] Nordlund (1984) holds a deviating view. However, the low-excitation lines lines he uses are not expected to have large δ_Γ values, according to Simmons & Blackwell (1982), and are therefore not good guides to the δ_Γ required by high-excitation lines.
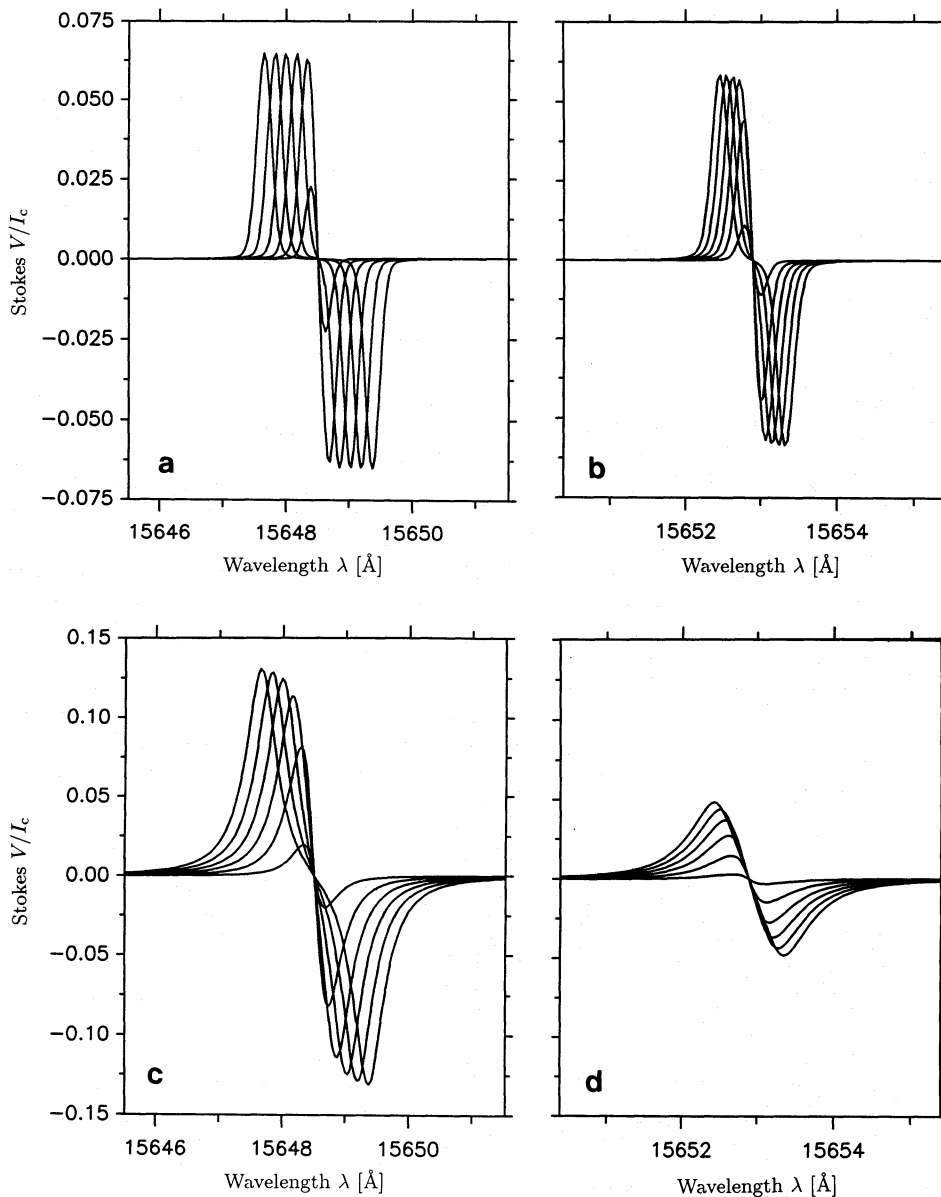
Fig. 4. Stokes V profiles of Fe I 15648.5 Å (Figs. 4a and c) and of Fe I 15652.9 Å (Figs. 4b and d) for the atmospheres NET (Figs. 4a and b) and MALTM (Figs. 4c and d). In each frame the profiles for a height-independent field strength of 100, 500, 1000, 1500, 2000 and 2500 G at an inclination $\gamma = 0°$ are shown. Note the difference between the vertical scales of Figs. 4a and b, on the one hand, and of Figs. 4c and d, on the other. All profiles have been convolved with a Gaussian macroturbulent velocity distribution of width $\xi_{mac} = 2$ km/s. The fudge-factor to the Van der Waals damping constant – $\delta_\Gamma = 2.5$

have to be broadened either by a velocity well over 5 km/s rms, or else by a broad distribution of field strengths, between 2000 and 4800 G for $\delta_\Gamma = 1.5$, or between 2400 and 4400 G for $\delta_\Gamma = 2.5$. All cases give equally good fits (see Rüedi 1991 for more details), but also appear rather far-fetched. Beckers (1976) finds a macroturbulence broadening of only 1–2 km/s in umbrae, while, e.g., Lites et al. (1991) find no evidence for large fluctuations of the field strength on small spatial scales in umbrae. Therefore, we have also attempted to fit the observed Stokes V profiles with a cooler model, the umbral model E of Maltby et al. (1986, MALTE), describing the dark part of umbrae during the early phase of the 11-year sunspot cycle. Now the observed profile is well reproduced with a much narrower field-strength distribution ranging from 3300 G to 3700 G (for $\delta_\Gamma = 2.5$), which appears much more realistic. If $\delta_\Gamma = 1.5$ is assumed, then a temperature even cooler than MALTE is required in order to reproduce the observed profile without having to postulate a substantial horizontal variation of the field strength. For the calculations in papers III, IV and V we therefore use $\delta_\Gamma = 2.5$.

3.2. Magnetic field strength and Zeeman splitting

Figure 6a shows the wavelength separation, $\Delta\lambda_{max}$, between the blue and red Stokes V peaks (upper set of curves: $g_{eff} = 3$ line, lower set: $g = 1.53$ line). For each line 4 different curves are plotted, one each for the models NET and DF and two for the MALTM atmosphere (one each for $\delta_\Gamma = 1.5$ and 2.5). The curves are labelled in the figure. All the profiles have been convolved with a macroturbulence of 2 km/s. The angle of inclination of the field, γ, is 0°. The curves for the other 3 models (PLA, HSRASP and OS2) are almost indistinguishable from the NET curves.

For sufficiently strong fields $\Delta\lambda_{max}$ reacts linearly to any field strength changes, as expected for a completely Zeeman split line. In the NET model the $g = 3$ line is completely split for $B \gtrsim 500$ G, and the $g_{eff} = 1.53$ line for $B \gtrsim 1000$ G, in accordance with its lower g_{eff} value. Due to the considerably larger non-magnetic width of the lines in the MALTM atmosphere (compare panels c and d of Fig. 4 with panels a and b) the lines are completely Zeeman split only for much larger B (1500 G for
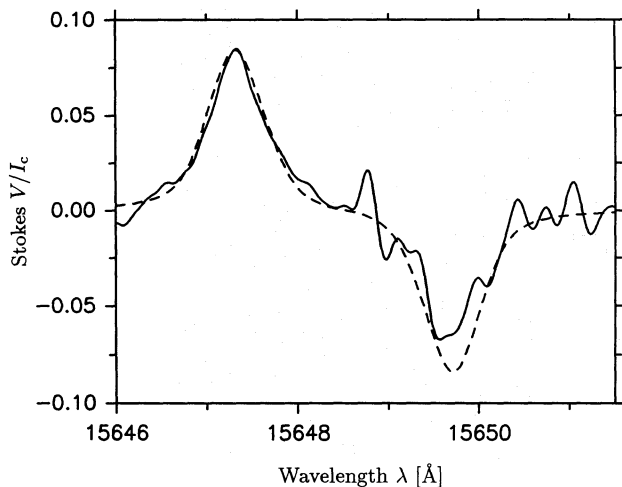
Fig. 5. Stokes V profiles of the $g = 3$ line. Solid curve: Spectrum observed in the darkest part of a large sunspot umbra. Note the numerous weak molecular blends, particularly in the red half of the line. Dashed curve: Profile calculated in the MALTM atmosphere for a distribution of field strengths centred on 3500 G and ranging from 2000 G to 4800 G. $\delta_\Gamma = 1.5$ and angle of inclination $\gamma = 0°$. No stray-light correction was necessary

the $g = 3$ line, although its sensitivity to lower field strengths is not greatly diminished).[2] Note that even for the most Zeeman sensitive lines in the visible the completely Zeeman split regime is only reached at field strengths 1.5 times larger than those at which the $g_{eff} = 1.53$ line becomes completely split.

We have also tested the influence of other atmospheric parameters on the Zeeman splitting. The angle of inclination of the field, γ, has an almost negligible influence on the $\Delta\lambda_{max}$ vs. B curves. The microturbulence, when varied within reasonable limits, also has little influence on $\Delta\lambda_{max}$. Only the macroturbulence, ξ_{mac}, shows some effect. Figure 6b shows $\Delta\lambda_{max}$ vs. B for the NET atmosphere and 3 different ξ_{mac} values. A Gaussian distribution of macroturbulent velocities is assumed. A larger ξ_{mac}, since it increases the line width, causes the strong-field limit to be reached for higher field strengths. For a profile completely unbroadened by any ξ_{mac} the $g = 3$ line in the NET atmosphere is already completely split at 300–400 G.

With the help of Figs. 6a and b the errors introduced by uncertainties in the atmospheric parameters into B values measured using $\Delta\lambda_{max}$ can be judged. If some rough estimate of the temperature and the macroturbulence (2 km s^{-1} appears to be reasonable in most cases, see Papers I, III and V) can be made, then Fig. 6 may serve as a calibration for the accurate measurement of (height-independent) field strengths $\gtrsim$ 500 G. Of course, for data affected by broad instrumental profiles the influence of the instrument has to be taken into account additionally.

3.3. Magnetic field strength and the Q/V ratio

The ratio $\sqrt{Q^2 + U^2}/V$ provides the most direct diagnostic of the magnetic inclination angle γ relative to the line of sight. At suffi-

---

[2]   A spectral line is completely Zeeman split when $\Delta\lambda_H / \Delta\lambda_D \gtrsim 1$, i.e. when the Zeeman splitting, $\Delta\lambda_H$, is larger than the "non-magnetic" width of the line, $\Delta\lambda_D$, which includes Doppler broadening, broadening due to turbulent velocity, line saturation, damping, etc.

ciently large field strengths the σ-component amplitudes of V, Q and U (V_{max}, Q_{max} and U_{max}, respectively) are all independent of B. In this regime γ may be determined from $\sqrt{Q^2 + U^2}/V$ without an explicit knowledge of the field strength. For small B, on the other hand, $V \sim B$, while Q, $U \sim B^2$, so that $\sqrt{Q_{max}^2 + U_{max}^2}/V_{max}$ depends not only on γ but also linearly on field strength. An error in the assumed field strength can lead to substantial errors in the derived γ (Stenflo 1985). Furthermore $\sqrt{Q^2 + U^2}$ runs the risk of being easily drowned in the noise for small B. In Fig. 7 $\sqrt{Q_{max}^2 + U_{max}^2}/V_{max}$ is plotted for both lines, calculated at $\gamma = 51.8°$ in the two extreme models NET and MALTM. $\delta_\Gamma = 2.5$ and an azimuthal angle of the field, $\chi = 0°$ has been chosen. Note how much quicker $\sqrt{Q_{max}^2 + U_{max}^2}/V_{max}$ reaches its asymptotic value for the $g = 3$ line than for the $g_{eff} = 1.53$ line. Also note that $\sqrt{Q_{max}^2 + U_{max}^2}/V_{max}$ still depends on B at field strengths at which, according to Fig. 6, the V profile is already completely split. This is due to the presence of a π-component in Stokes Q and U, which hampers these profiles from becoming completely split. The main advantage of Fe I 15648.5 Å is that, at least outside umbrae, $\sqrt{Q_{max}^2 + U_{max}^2}/V_{max}$ depends only on γ and not on B, as long as $B \gtrsim$ 1000 G. This greatly simplifies the determination of γ. In the umbra $\sqrt{Q_{max}^2 + U_{max}^2}/V_{max}$ becomes independent of the field strength only for $B \gtrsim$ 2500 G.

Since the shape of the curves in Fig. 7 does not change significantly with γ, they can be used to calibrate observed $\sqrt{Q_{max}^2 + U_{max}^2}/V_{max}$ ratios in order to determine γ.[3] The curves for other γ values differ from the plotted ones mainly by the factor $\sin^2\gamma / \cos\gamma$.

The relatively large $\sqrt{Q_{max}^2 + U_{max}^2}/V_{max}$ ratio of Fe I 15648.5 Å, as compared to less Zeeman sensitive lines also has a disadvantage. The influence of cross-talk from Stokes Q and U into Stokes V due to the non-diagonal terms in the Mueller matrix of the telescope is proportional to the Stokes Q und U signals present. Larger Stokes Q and U therefore also enhance the instrumental cross-talk into V. However, since the Stokes profiles of the $g = 3$ line are expected to satisfy the theoretical symmetry properties of Stokes profiles for a static atmosphere to a high degree (Grossmann-Doerth et al. 1989), the method outlined by November (1991) to remove this cross-talk may be applied if all 4 Stokes parameters are measured.

3.4. Magnetic field strength and line ratio

The peak separation $\Delta\lambda_{max}$ of the $g = 3$ line ceases, on its own, to be a reliable indicator of the field strength below $B \approx$ 500–1000 G, with the exact value of the critical field depending on the atmosphere. By fitting the whole V profile of the line this limit can be lowered at the most to 300–600 G. In order to obtain even lower field strengths the ratio between the Stokes V profiles of the two lines must be analysed. A line ratio as a reliable field-strength diagnostic (magnetic line ratio, or MLR) was first introduced by Stenflo (1973) between two lines in the visible (Fe I 5250.2 Å, $g = 3$, and Fe I 5247.1 Å, $g_{eff} = 2$). The ratio between the V profiles of 2 lines, which have different Zeeman sensitivities but are otherwise similar, is a function of field strength, as may be seen from Fig. 8 in which

---

[3]   Recall, however, that Q and U react more strongly to macroturbulent and instrumental broadening than V (Solanki et al. 1987).
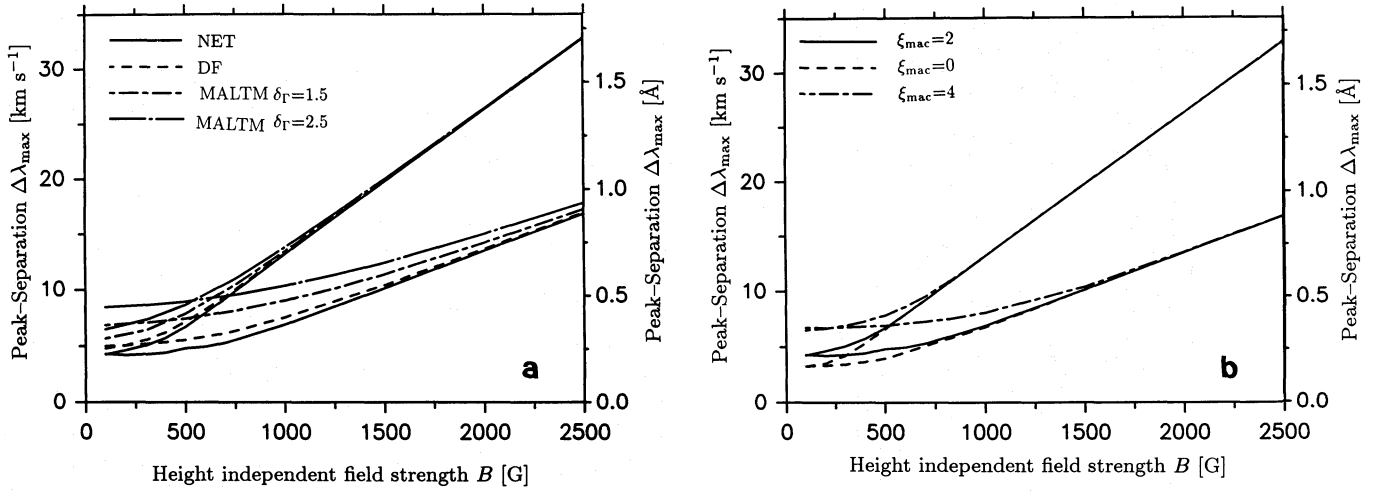
318

Fig. 6. Wavelength separation, $\Delta\lambda_{max}$, between the red and blue Stokes V peaks vs. height-independent field strength, B. The upper set of curves refers to the Fe I 15648.5 Å (g = 3) line, the lower set to Fe I 15652.9 Å (g_{eff}= 1.53). **a.** Dependence of $\Delta\lambda_{max}$ on temperature. The individual curves in each set represent either different model atmospheres, or δ_Γ values, as identified in the figure. The curves marked NET also represent the results of the PLA, HSRASP and OS2 atmospheres. ξ_{mac} = 2 km/s, γ = 0°. **b.** Dependence of $\Delta\lambda_{max}$ on macroturbulence ξ_{mac}. Three ξ_{mac} values have been tested, 0, 2 and 4 km/s. The plotted curves were calculated using the NET atmosphere, δ_Γ = 2.5 and γ = 0°

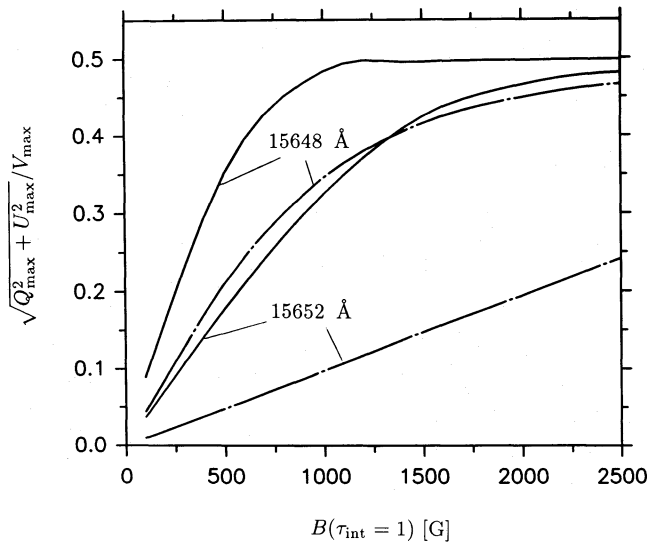**Fig. 7.** Ratio of the $\sqrt{Q^2 + U^2}$ amplitude (of the σ-components) to Stokes V amplitude, $\sqrt{Q^2_{max} + U^2_{max}}/V_{max}$ for the models NET (solid curves) and MALTM (dot-dashed curves). δ_Γ = 2.5 and γ = 51.8°. The curves for the two lines are marked in the figure

Fig. 8. Weighted ratio of the Stokes V amplitudes of the two lines: 1.53 $V_{max}(15648)/(3V_{max}(15652))$, vs. height-independent magnetic field strength B. The 3 curves represent the line ratio resulting from 3 different models: NET, HSRASP and OS2

$$MLR = \frac{g_{eff}(15652)\,V_{max}(15648)}{g(15648)\,V_{max}(15652)} = \frac{1.53\,V_{max}(15648)}{3\,V_{max}(15652)}$$

is plotted as a function of field strength B. The 3 curves represent the MLR in 3 different model atmospheres. Note the rapid decrease of the MLR with field strength, as the amplitude of the Stokes V profile of the g = 3 line begins to saturate, while that of the g_{eff} = 1.53 line still continues to increase. For larger B the MLR begins to level off again as the g_{eff} = 1.53 line also becomes completely split.

If the temperature is known then field strengths as low as 100 G can be measured with this line pair with an accuracy
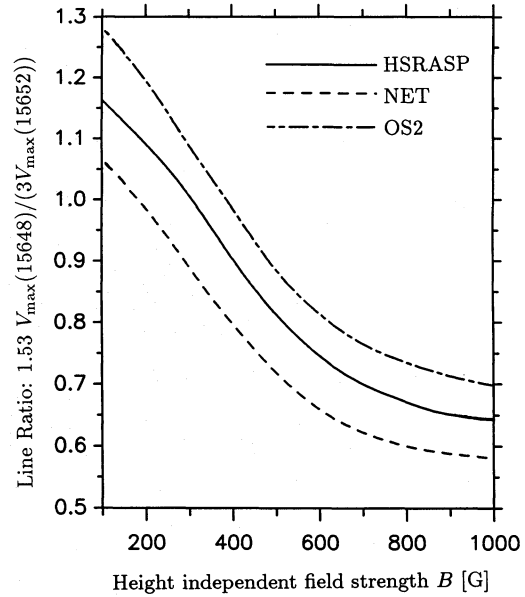
determined essentially by the signal-to-noise in the data. In the absence of an additional, sensitive temperature diagnostic the uncertainty in the field strength derived from the line ratio is approximately 100–150 G, if a rough idea of the type of feature observed is present (e.g. umbra, penumbra, pore, plage). The uncertainty may be judged by considering the difference between the 3 curves in Fig. 8. This suggests that the investigated line pair, although reasonably suited to form a MLR, is not ideal. It should be well worthwhile to look for a replacement for Fe I 15652.9 Å that also has a g_{eff} value below 2, but is otherwise more similar to Fe I 15648.5 Å. Fe I 15822.8 Å is an interesting

candidate (Zayer et al. 1989), but is hampered by the proximity of a neighbouring line to its blue wing.

3.5. Magneto-optical effects and the Stokes V profile

Some of the Stokes V profiles observed by Livingston (1991) show a reversal near line centre reminiscent of magneto-optical effects. One such profile is exhibited in Fig. 9a. To test this hypothesis we have looked through all our calculated profiles (i.e. the full grid of temperatures, field strengths and inclination angles) to find the V profile with the largest inversion in its core. This profile, an outcome of calculations in the DF model for $B = 2000$ G and $\gamma = 50°$, is plotted in Fig. 9b before (solid curve) and after (dashed curve) broadening with a macroturbulence of 2 km/s.[4] Magneto-optical effects are obviously unable to explain the observed inversions. For a model that is more successful in reproducing such profiles see Paper III.
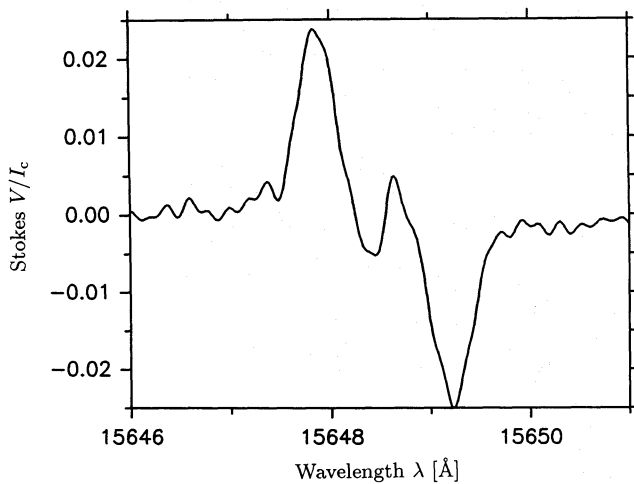

Fig. 9a. Stokes V profile of the $g = 3$ line observed in an active region plage. Note the inversion near the line core

4. Results based on flux-tube models

The Stokes V profile shape of the $g = 3$ line observed in plages is best reproduced by flux-tube models (Zayer et al. 1989). Since the plage observations we analyse in papers III and IV were all obtained near disk centre and since flux tubes are expected to be vertical (Schüssler 1986) we need discuss only Stokes V. All the test calculations have been carried out with a filling factor α of 0.05. Since small flux tubes are generally warm we have only considered two models, the HSRASP (always denoted by a solid curve in the figures) and PLA (always plotted dashed).

---

[4]   Later calculations with the MALTM model show equally large or even larger magneto-optical inversions at field strengths greater than 3000 G, but such B values are much too large to explain the observed plage profiles.
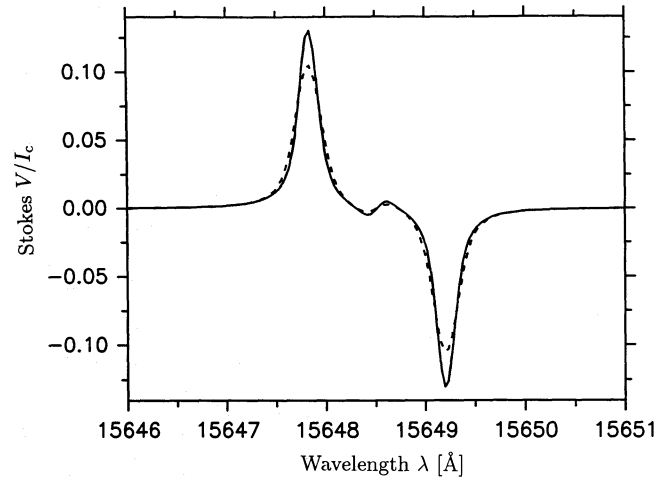

Fig. 9b. Synthetic Stokes V profiles of the $g = 3$ line. The plotted profiles show the largest inversion due to magneto-optical effects of all the calculated profiles in the model grid. The DF model (Ding and Fang 1989), a height-independent field strength of 2000 G and an inclination angle of 50° were used. Solid curve: $\xi_{mac} = 0$ km/s, dashed curve: $\xi_{mac} = 2$ km/s

4.1. Magnetic field strength: Zeeman splitting

Figure 10 shows the Stokes V peak separation, $\Delta\lambda_{max}$, vs. $B(\tau_{int} = 1)$. The conversion to $B(z = 0)$ for either model can be made using Fig. 3. The overall impression given by Fig. 10 is qualitatively similar to Fig. 6, but differs considerably in detail. For example, the transition from the weak-field limit, in which $\Delta\lambda_{max}$ remains essentially unaffected by the field strength into the strong-field regime is made at larger field strengths than in the case of a height-independent field. There are two main reasons for this. Firstly, the lines are formed above $\tau_{int} = 1$, at a height at which the field strength is generally 10–20% lower than at $B(\tau_{int} = 1)$, but see below. Secondly, due to the presence of a field strength gradient, the individual σ-components are broadened (see Sect. 4.2), so that it requires larger field strengths to separate them completely. In the HSRASP the $g = 3$ line is completely split for $B(\tau_{int} = 1) \gtrsim 800$–1000 G, while in the PLA model this is only the case beyond 1300–1500 G. The slower increase of $\Delta\lambda_{max}$ with $B(\tau_{int} = 1)$ for PLA can be explained as follows. For small $B(\tau_{int} = 1)$ the temperature and consequently the pressure-scale height inside the flux tube becomes larger than outside at equal geometrical height. Since the pressure difference at $z = 0$ is small for the two models, the gas pressure inside the tube, p_{int}, becomes larger than the gas pressure outside, p_{ext}, not far above $z = 0$. Just below this critical height, at which $p_{int} = p_{ext}$, the field expands very rapidly to fill the available space, thus forming a magnetic canopy (see Solanki & Steiner 1990, for more details). This effect is quite evident in the $B(z)$ function of the plage model with $B(\tau_{int} = 1) = 500$ G shown in Fig. 3b. The critical height in that example is reached at $z \approx 110$ km. Therefore for the PLA model at small $B(\tau_{int} = 1)$ the lines are formed above the canopy base in a field strength smaller than $B(\tau_{int} = 1)$ by a factor of 10–20.

Figure 10 differs from Fig. 6 also in the strong field regime. For the thin-tube model $\Delta\lambda_{max}(B)$ does not asymptotically approach a straight line, but follows a curved path. A part of the deviation from a straight line is due to the fact that as the line becomes increasingly split the wavelength of the Stokes V maximum is formed increasingly higher in the atmosphere, where the magnetic field strength is smaller. Another, possibly larger, part
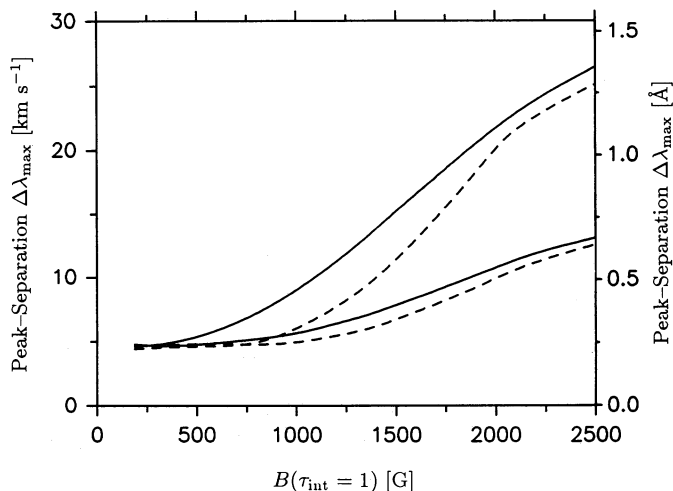
Fig. 10. Wavelength separation between the Stokes V peaks, $\Delta\lambda_{max}$, vs. the field strength at unit continuum optical depth within the flux tube, $B(\tau_{int} = 1)$. The calculations were carried out at solar disk centre for vertical thin-tube models having the HSRASP (solid curves) and PLA (dashed curves) atmospheres within the flux tube. The non-magnetic surroundings are described by the HSRASP. The upper two curves represent Fe I 15648.5 Å, the lower two Fe I 15652.9 Å. $\zeta_{mac} = 2$ km/s

is due to the fact that the pressure scale height (i.e. dB/dz) varies non-linearly with depth, so that the field strength at $\tau_{int} = 1$ and at the height of line formation are not coupled linearly (cf. Fig. 3b).

4.2. Magnetic field strength gradient and σ-component width

For a height-independent field the width of the σ-component of the Stokes V profile, $\Delta\lambda_{FWHM}$, depends on the field strength only for incompletely split lines, for which the 2 σ-components partly overlap. The maximum σ-width achieved for a height-independent field is 5.2 km/s for PLA and 6.2 km/s for the HSRASP. In contrast, for a magnetic field satisfying horizontal pressure balance the line width depends on the field strength even for large B (compare $\Delta\lambda_{FWHM}$ plotted in Fig. 11 with the peak separation in Fig. 10). The reason for the large σ-width is, of course, the vertical gradient of the field strength present in the current models (Zayer et al. 1989). The difference between the solid and the dashed curve below $B(\tau_{int} = 1) \approx 1000$ G has the same causes as the difference seen in Fig. 10.

As $B(\tau_{int} = 1)$ is increased by shifting the internal atmosphere downwards the height of line formation approaches the level at which the temperature gradient of the external atmosphere is steepest. Due to the higher temperature (i.e. pressure scale height) the field-strength gradient then does not increase so rapidly with increasing $B(\tau_{int} = 1)$. For the PLA model with its lower temperature gradient this effect can even lead to a decrease of $dB/d\tau$ at the height of line formation as $B(\tau_{int} = 1)$ is increased, explaining the behaviour of the dashed curve for $B(\tau_{int} \approx 1) \gtrsim 1900$ G.

Note that for typical flux-tube field strengths [$B(\tau_{int} = 1) \approx 2000$–$2500$ G] the curves of the two models in Fig. 11 differ by, in general, less than 10%. Therefore, both models should reproduce $\Delta\lambda_{FWHM}$ of observed V profiles almost equally well. Recall, however, that this need not be the case for all empirical flux-tube models. For example, the empirical models of Keller
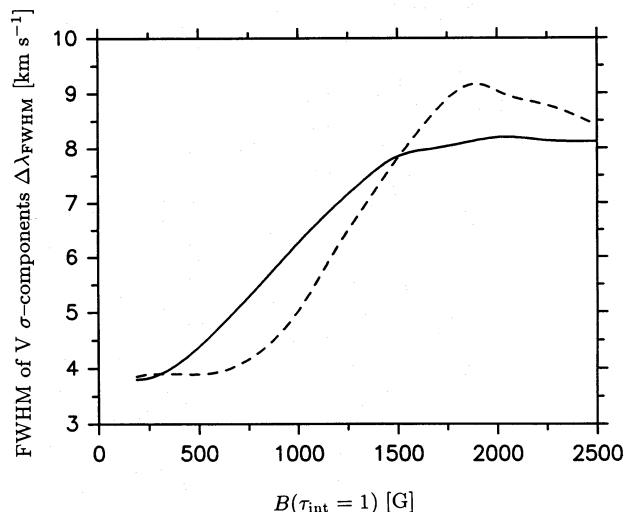

Fig. 11. Full width at half maximum ($\Delta\lambda_{FWHM}$) of the Stokes V σ-components of the $g = 3$, line Fe I 15648.5 Å, vs. $B(\tau_{int} = 1)$. The models are the same as in Fig. 10

et al. (1990) give a considerably narrower $\Delta\lambda_{FWHM}$ of the $g = 3$ line. Since the temperature stratification below log $\tau_{int} = -1$ of empirical models is rather uncertain (Paper I) $\Delta\lambda_{FWHM}$ remains relatively model dependent.

4.3. Magnetic field strength and line ratio

Figure 12 shows the MLR of the two infrared lines vs. $B(\tau_{int} = 1)$ for the same models as discussed in Sects. 4.1 and 4.2. Again, the qualitative behaviour is similar to the height-independent field case, but the details are different. Most noticeable is the reduced sensitivity of the MLR for the thin-tube models. This has partly to do with the increased line widths due to the vertical field-strength gradient, but probably to a larger extent with the fact that B at the height of line formation is smaller than $B(\tau_{int} = 1)$. This is particularly true for the PLA model (see Sect. 4.1 and compare Fig. 12 with Fig. 10). Figure 12 reinforces the need for a replacement for Fe I 15652.9 Å aimed at making the line ratio less temperature dependent. Since we expect the HSRASP to be a better representation of the temperature within weak-field features, it should nevertheless be possible to measure fields as low as $B(\tau_{int} = 1) \approx 200$–$250$ G, for thin flux tubes with high-quality data. Again, this is similar to values achievable with the 12 μm lines.

For strong fields the σ-components of the $g = 3$ line are broadened more strongly than those of the $g_{eff} = 1.53$ line due to the magnetic gradient. This can lead to a continuing reduction of the line ratio to well below the values expected for the strongest height-independent fields.

The use of a line ratio, when combined with the analysis of the complete V profiles, can even allow us to distinguish between horizontal and vertical magnetic field gradients using only 2 well-chosen infrared lines. The basic idea behind the proposed diagnostic is the fact that a longitudinal field gradient not only broadens the σ-components of a Zeeman sensitive line, it also increases the equivalent width of its σ-components. This is simply another twist to the well-known Zeeman-desaturation effect: The total equivalent width of a saturated Zeeman-split spectral line is increased, due to the distribution of the absorption
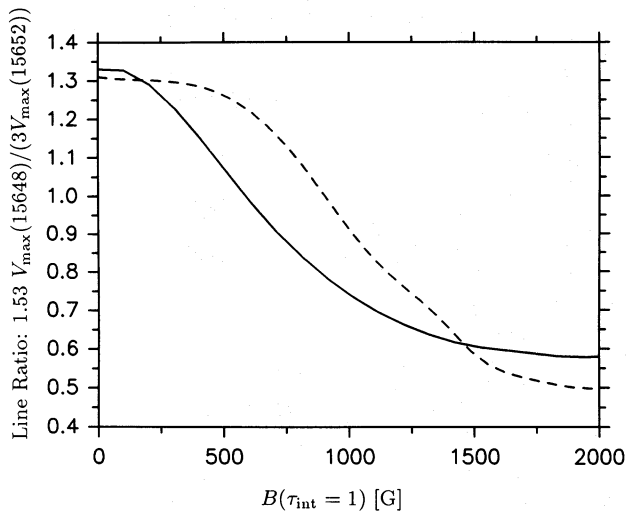
Fig. 12. Line ratio $1.53 \times V_{max}(15648)/(3 \times V_{max}(15652))$ vs. $B(\tau_{int} = 1)$ for the same flux-tube models as in Fig. 10

over a larger wavelength interval produced by the presence of a separated σ- and π-components. Similarly, a longitudinal field-strength gradient increases the W_λ of each σ-component, since it increases the wavelength range over which it absorbs. For two lines with different, but complete Zeeman splittings, a longitudinal B-gradient therefore increases W_λ of their σ-components by different amounts.[5] Thus if either the temperature is known, or if both lines have the same temperature sensitivity then the ratio of the *areas* of the σ-components of the two lines allows us to distinguish between horizontal and vertical gradients of B.

5. Conclusions

In this, the second of a series of papers on infrared spectral lines and magnetic fields, we have studied the properties and the diagnostic potential, of two spectral lines in the infrared H-band, namely Fe I 15648.5 Å with $g = 3$ and Fe I 15652.9 Å with $g_{eff} = 1.53$.

We find, in agreement with Paper I, that they are not very sensitive to plage-like temperatures and can, therefore, constrain the temperature in small-scale magnetic features only very poorly. On the other hand, the small temperature sensitivity increases the reliability of these lines for magnetic field measurements. Due to their increased sensitivity to cool tempeatures the 2 lines may be able to constrain the temperature in sunspot umbrae, although blending by molecular lines can become a problem.

Tests of the magnetic sensitivity of these lines show that height-independent field strengths as low as 300 G (for not too cool atmospheres) can be measured from the splitting of the σ-components of the Stokes V profiles. For thin-tube magnetic fields the corresponding limit is approximately 400–500 G (for the HSRASP) to 800–900 G (for PLA) at $\tau_{int} = 1$. By introducing the ratio between the V profiles of the two lines the smallest mea-

---

[5] For very large field strengths with very large gradients the splitting pattern becomes more important than the effective Landé factor of a line (Basri et al. 1992), but these field strengths are larger than generally found in solar flux tubes.

surable field strength is lowered to approximately 100 G for the height-independent field and to approximately 200–250 G for the thin-tube model (HSRASP atmosphere).

Field strengths as low as this were previously thought to be measurable only with the $g = 1$ Mg I emission lines at 12μ, which have a magnetic sensitivity that is approximately 2.7 times larger than of the $g = 3$ Fe I 15648.5 Å. With the help of the Stokes V line ratio the sensitivity of the 1.5μ lines can be increased by a factor of 2.5–3 beyond that achievable from the splitting alone, thus reaching the level of the 12μ lines. Since the two strongest unblended 12μ emission lines, the only ones currently observable with sufficient S/N, both have $g = 1$ (Lemoine et al. 1988), constructing a similar line ratio between them does not increase their sensitivity to the field strength.

One major difference between the 15648 Å and the 12μ lines is that the latter are formed in the upper photosphere near the temperature minimum (Deming et al. 1988; Lemke & Holweger 1987; Carlsson et al. 1992; Chang et al. 1991), while the 1.5μ lines are formed very deep in the photosphere. Our calculations give maxima of the line depression contribution functions at the wavelengths of the Stokes V peaks between $\log \tau = -0.5$ and -1.5. Thus the lines in the two wavelength ranges sample the field strength at two different heights, so that they can be combined to make a (limited) 3-D map of the magnetic field strength in the solar photosphere. But this is not the only consequence of the different heights of formation. In small-scale magnetic features the field strength can decrease by a factor of 4–8 between the heights of formation of the 1.5μ and the 12μ lines due to pressure balance in the stratified solar atmosphere. Therefore the 1.5μ lines may actually be able to measure the field strength in magnetic features for which the 12μ lines can only give upper limits. Similarly, the 1.5μ lines should, in principle, also give smaller relative errors for the field strengths in small-scale magnetic features.

The $g = 3$ Fe I 15648.5 Å line is found to be a good candidate for determining the inclination angle of the magnetic field due to its large Stokes Q and U profiles even for relatively small Zeeman splittings and due to the field-strength independence of the $\sqrt{Q_{max}^2 + U_{max}^2}/V_{max}$ ratio for B $\gtrsim 1000$ G. Finally, we have also investigated the importance of magneto-optical effects and find that these are unable to explain one of the prominent features of some of the observed Stokes V profiles, namely an inversion near the core of the $g = 3$ line (Livingston 1991). In Paper III we analyse the cause of such inversions and other distortions of the observed V profiles in detail.

References

Basri G., Marcy G.W., Valenti J.A., 1992, ApJ in press

Beckers J.M., 1976, ApJ 203, 739

Carlsson M., Rutten R.J., Shchukina N.G., 1992, A& A 253, 567

Chang E.S., Avrett E.H., Mauas P.J., Noyes R.W., Loeser R., 1991, ApJ 379, L79

Delbouille L., Roland G., Brault J.W., Testerman L., 1981, *Photometric Atlas of the Solar Spectrum from 1850 to 10 000 cm⁻¹*, NOAO, Tucson, Az.

Deming D., Boyle R.J., Jennings D.E., Wiedemann G., 1988, ApJ 333, 978

322

Ding M.D., Fang C., 1989, A& A 225, 204

Giampapa M.S., Golub L., Worden S.P., 1983, ApJ 268, L121

Gingerich O., Noyes R.W., Kalkofen W., Cuny Y., 1971, Sol. Phys. 18, 347

Gondoin P., Giampapa M.S., Bookbinder J.A., 1985, ApJ 297, 710

Grossmann-Doerth U., Schüssler M., Solanki S.K., 1989, A& A 221, 338

Hall D.N.B., 1974, *An Atlas of Infrared Spectra of the Solar Photosphere and of Sunspot Umbrae*, Kitt Peak National Observatory, Contribution No. 556, Tucson, AZ.

Harvey J.W, 1977, in *Highlights of Astronomy*, E.A. Müller (Ed.), Vol. 4, Part II, p. 223

Harvey J.W., Hall D., 1975, *Bull. Amer. Astron. Soc.* **7**, 459.

Holweger H., 1979, in *Proc. 22nd Liège International Astrophys. Symp.*, Inst. d'Astrophysique, Liège, p. 117

Johansson S., Learner R.C.M., 1990, ApJ 354, 755

Keller C.U., Solanki S.K., Steiner O., Stenflo J.O., 1990, A& A 233, 583

Knölker M., Schüssler M., Weisshaar E.: 1988, A& A 194, 257

Lemke M., Holweger H., 1987, A& A 173, 375

Lemoine B., Demuynck C., Destombes J.L., 1988, A& A 191, L4

Lites B.W., Bida T.A., Johannesson A., Scharmer G.B., 1991, ApJ 373, 683

Livingston W., 1991, in Solar Polarimetry, L. November (Ed.), National Solar Obs., Sunspot, NM, p. 356

Maltby P., Avrett E.H., Carlsson M., Kjeldseth-Moe O., Kurucz R.L., Loeser R., 1986, ApJ 306, 284

Muglach K., Solanki S.K., 1992, A&A 263, 301 (Paper I)

Murphy G.A., 1990, NCAR Cooperative Thesis No. 124

Murphy G.A., Rees D.E., 1990, *Operation of the Stokes Profile Synthesis Routine*, NCAR Technical Note, NCAR/TN-348+IA

Nordlund Å., 1984, in *Small–Scale Dynamical Processes in Quiet Stellar Atmospheres*, S.L. Keil (Ed.), National Solar Obs., Sunspot, NM, p. 181

November L.J., 1991, in Solar Polarimetry, L. November (Ed.), National Solar Observatory, Sunspot, NM, p. 149

Obridko V.N., Staude J., 1988, A& A 189, 232

Rabin D., 1991, ApJ 391, 832

Rabin D., Jaksha D., Plymate C., Wagner J., Iwata K., 1991, in Solar Polarimetry, L. November (Ed.), National Solar Observatory, Sunspot, NM, p. 361

Rees D.E., Murphy G.A., Durrant C.J., 1989, ApJ 339, 1093

Rüedi I., 1991, Diplomarbeit, ETH Zürich

Rüedi I., Solanki S.K., Livingston W., Stenflo J.O., 1992a, A& A submitted (Paper III)

Rüedi I., Solanki S.K., Rabin D., 1992b, A&A 261, L21 (Paper IV)

Schüssler M., 1986, in *Small Scale Magnetic Flux Concentrations in the Solar Photosphere*, W. Deinzer, M. Knölker, H.H. Voigt (Eds.), Vandenhoeck & Ruprecht, Göttingen, p. 103

Simmons G.J., Blackwell D.E., 1982, A& A 112, 209

Solanki S.K., 1986, A& A 168, 311

Solanki S.K., Biémont E., Mürset U., 1990, A& AS 83, 307

Solanki S.K., Keller C., Stenflo J.O., 1987, A& A 188, 183

Solanki S.K., Roberts B., 1992, MNRAS 256, 13

Solanki S.K., Rüedi I., Livingston W.C., 1992, A&A 263, 339 (Paper V)

Solanki S.K., Steiner O., 1990, A& A 234, 519

Spruit H.C., 1974, Sol. Phys. 34, 277

Steiner O., Pizzo V.J., 1989, A& A 211, 447

Stenflo J.O., 1973, Sol. Phys. 32, 41

Stenflo J.O., 1985, in *Measurements of Solar Vector Magnetic Fields*, M.J. Hagyard (Ed.), NASA Conf. Publ. 2374, p. 263

Stenflo J.O., Solanki S.K., Harvey J.W., 1987, A& A 173, 167

Sun W.-H., Giampapa M.S., Worden S.P., 1987, ApJ 312, 930

Unsöld A., 1955, *Physik der Sternatmosphären*, Springer Verlag, Berlin

Zayer I., 1989, *Ph.D. Thesis*, No. 8995, ETH, Zürich

Zayer I., Solanki S.K., Stenflo J.O., 1989, A& A 211, 463

Zayer I., Solanki S.K., Stenflo J.O., Keller C.U., 1990, A& A 239, 356